

Correlation Effects on Charge Order and Zero-Gap State in the Organic Conductor α -(BEDT-TTF) $_2$ I $_3$

Yasuhiro Tanaka¹ and Masao Ogata²

¹*Department of Physics, Chuo University, Bunkyo, Tokyo 112-8551, Japan*

²*Department of Physics, University of Tokyo, Bunkyo, Tokyo 113-0033, Japan*

The effects of electron correlation in the quasi-two-dimensional organic conductor α -(BEDT-TTF) $_2$ I $_3$ are investigated theoretically by using an extended Hubbard model with on-site and nearest-neighbor Coulomb interactions. A variational Monte Carlo method is applied to study its ground-state properties. We show that there appears a nonmagnetic horizontal-stripe charge order in which nearest-neighbor correlation functions indicate a tendency toward a spin-singlet formation on the bonds with large transfer integrals along the charge-rich stripe. Under uniaxial pressure, a first-order transition from the nonmagnetic charge order to a zero-gap state occurs. Our results on a spin correlation length in the charge-ordered state suggest that a spin gap is almost unaffected by the uniaxial pressure in spite of the suppression of the charge disproportionation. The relevance of these contrasting behaviors in spin and charge degrees of freedom to recent experimental observations is discussed.

1. Introduction

Low-dimensional organic conductors have been studied intensively.¹ They exhibit intriguing electronic phases that originate from a variety of their crystal structures and strong Coulomb interactions among electrons.² Typical examples are Mott insulators and charge-ordered states in which the effects of electron correlation play an important role in understanding their physical properties.

Among various compounds, the quasi-two-dimensional organic conductor α -(BEDT-TTF) $_2$ I $_3$ [BEDT-TTF=bis(ethylenedithio)tetrathiafulvalene], which we abbreviate as α -I $_3$ hereafter, has attracted much attention.³ It shows a metal-insulator transition at $T_{CO} = 135$ K,⁴ which is of first order with a small structural distortion.⁵⁻⁷ The conduction layer of α -I $_3$ consists of donor BEDT-TTF molecules and forms a 3/4-filled band since the anion I $_3^-$ is monovalent. Below T_{CO} , a horizontal-stripe charge order (CO) appears⁸⁻¹³ together with a spin-gap behavior as observed in the magnetic susceptibility measurement.¹⁴ By applying

uniaxial pressure, this CO changes into a zero-gap state (ZGS).¹⁵ Various anomalous transport phenomena observed in this ZGS³ are considered to originate from massless Dirac fermions¹⁶ located at the Fermi level in the energy dispersion.

Theoretically, several authors have investigated the physical properties of α -I₃ in its various electronic phases including the CO,^{17–21} superconductivity,^{22,23} and the ZGS.^{16,24–46} By using an extended Hubbard model, Kobayashi *et al.* have found that the CO becomes unstable and the ZGS appears with increasing uniaxial pressure,²³ the effect of which is incorporated in the modification of transfer integrals. They have also shown that the peculiar network of transfer integrals in this compound is crucially important for the realization of the Dirac-type energy dispersion.¹⁶ Although the above studies have explained some aspects of recent experimental findings,³ our understanding on this system is still limited in the sense that most of these theories are based on the mean-field approximation (MFA) that ignores electron correlation effects. For example, the MFA predicts an antiferromagnetic spin order in the CO,^{19,20,23,27} which is inconsistent with experiments showing the nonmagnetic CO below T_{CO} .¹⁴ The importance of the correlation effects is also suggested by an NMR study for $T > T_{\text{CO}}$.⁴⁷ Recent experiments under hydrostatic pressure have shown that the pressure dependences of the CO and the spin gap are considerably different from each other.^{48,49} Namely, the former is linearly suppressed until it disappears at around 10 kbar, whereas the latter is almost constant and steeply decreases near the phase boundary between the CO and the ZGS. Moreover, its effects on the massless Dirac fermions have not been fully explored yet.

With these facts in mind, we investigate the ground-state properties of α -I₃ by employing a variational Monte Carlo (VMC) method, which can take account of the quantum fluctuations. First, we show that a horizontal-stripe CO without the antiferromagnetic order is obtained for the first time, which is in contrast to the MFA. By increasing the uniaxial pressure, the nonmagnetic CO is suppressed and the ZGS becomes the ground state. In the CO state, nearest-neighbor spin-spin correlation functions indicate that a spin-singlet formation is favored on the bonds with large transfer integrals on the charge-rich stripe. This is because the magnitude of transfer integrals is alternating on the stripe, as pointed out by Seo¹⁹ within the MFA. The results are also consistent with the exact diagonalization study on small clusters with electron-phonon interactions²¹ that explicitly break the symmetry of the lattice. Furthermore, we show that the spin correlation length in the CO phase has very weak pressure dependence, which suggests the robustness of the spin gap. We discuss its origin and relevance to the experimental observations.^{48,49}

2. Model and Method

We consider the two-dimensional extended Hubbard model, which is written as

$$H = \sum_{\langle ij \rangle \sigma} t_{ij} (c_{i\sigma}^\dagger c_{j\sigma} + h.c.) + U \sum_i n_{i\uparrow} n_{i\downarrow} + \sum_{\langle ij \rangle} V_{ij} n_i n_j, \quad (1)$$

where $\langle ij \rangle$ represents a pair of neighboring sites, $c_{i\sigma}^\dagger$ ($c_{i\sigma}$) denotes the creation (annihilation) operator for an electron with spin σ at the i th site, $n_{i\sigma} = c_{i\sigma}^\dagger c_{i\sigma}$, and $n_i = n_{i\uparrow} + n_{i\downarrow}$. We consider a 1/4-filled system, which is equivalent to the 3/4-filled band for α -I₃ through a unitary transformation. The transfer integrals are written by t_{ij} , whereas U and V_{ij} indicate on-site and nearest-neighbor Coulomb interactions, respectively. The crystal structure of α -I₃ in the high-temperature metallic phase is schematically shown in Fig. 1. The unit cell contains four molecules, which we denote by A, A', B, and C. In the metallic phase, sites A and A' are equivalent to each other owing to the inversion symmetry, whereas they become inequivalent in the CO phase where sites A and B (A' and C) become charge-rich (charge-poor). Although the structural distortion slightly modulates the transfer integrals at T_{CO} , we do not take its effects into account for simplicity.^{20,21} For V_{ij} , we consider V_a and V_b on the vertical and diagonal bonds, respectively, as shown in Fig. 1.

We write the trial wave function for the VMC calculations as

$$|\Psi\rangle = P_W P_G |\Phi\rangle, \quad (2)$$

where $|\Phi\rangle$ indicates the wave function obtained by diagonalizing the mean-field Hamiltonian

$$H^{\text{MF}} = \sum_{\langle ij \rangle \sigma} t_{ij} (c_{i\sigma}^\dagger c_{j\sigma} + h.c.) + \sum_{\mu\alpha\sigma} \Delta_{\alpha\sigma} n_{\mu\alpha\sigma}, \quad (3)$$

where μ denotes the index for the unit cell and α is that for the site in the unit cell. P_G and P_W are projection operators for on-site and nearest-neighbor sites, respectively.^{50–53} They are defined as

$$P_G = \prod_i [1 - (1 - g)n_{i\uparrow}n_{i\downarrow}], \quad (4)$$

$$P_W = w_a^{\sum_{\langle ij \rangle_a} n_i n_j} w_b^{\sum_{\langle ij \rangle_b} n_i n_j}, \quad (5)$$

where $g \geq 0$, $w_a, w_b \leq 1$, and $\langle ij \rangle_a$ ($\langle ij \rangle_b$) stands for a pair of neighboring sites that are connected by the vertical (diagonal) bonds (see Fig. 1). The variational parameters $\Delta_{\alpha\sigma}$, g , w_a , and w_b are optimized by the stochastic reconfiguration method.⁵⁴ Typically, physical quantities are measured using $2\text{--}6 \times 10^5$ samples, which give sufficient statistical accuracy. In this paper, we do not consider any CO pattern with a unit cell which is different from that in Fig.

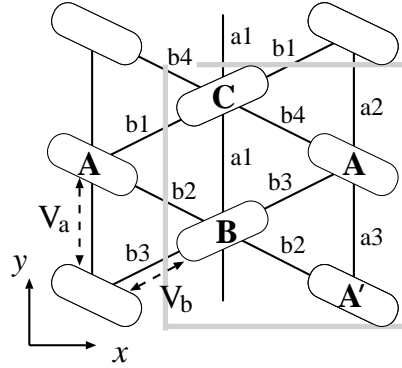


Fig. 1. Schematic representation of the crystal structure for α -I₃ in the metallic phase. The gray rectangle indicates the unit cell.

1.²⁰ For the transfer integrals, we use $t_{b1} = -0.127$, $t_{b2} = -0.145$, $t_{b3} = -0.062$, $t_{b4} = -0.025$, $t_{a1} = 0.035$, $t_{a2} = 0.046$, and $t_{a3} = -0.018$.¹¹ The unit of energy is eV hereafter. We take account of the effect of uniaxial pressure P (kbar) along the y -axis by modifying the transfer integrals t_{ij} as $t_i(P) = t_i(1 + K_i P)$ with K_i (eV/kbar) given in Ref. 22.

3. Results

3.1 Effects of P_G

Before discussing the results with fully optimized wave functions, we first examine the effects of P_G by setting $P_W = 1$ in Eq. (2). The values of $\Delta_{\alpha\sigma}$ are optimized. We use $U = 0.7$, $V_a = 0.35$, and $V_b = 0.25$ unless otherwise noted. Figure 2(a) shows the ground-state energy E_t as a function of g for $P = 0$ kbar. The system size is $N_u = L_x \times L_y = 8 \times 8$ with L_x (L_y) being a number of unit cells in the x -direction (y -direction). We show the average charge density $\langle n_{\alpha\sigma} \rangle$ in the unit cell in Figs. 2(b) and 2(c). For $g = 1$, the results are equivalent to those with the MFA,²⁰ which have CO together with antiferromagnetic order. We obtain a horizontal-stripe CO in which the sites A and B (A' and C) are charge-rich (charge-poor). In this state, we have $\langle n_{A\uparrow} \rangle > \langle n_{A\downarrow} \rangle$ and $\langle n_{B\downarrow} \rangle > \langle n_{B\uparrow} \rangle$ so that the spins on the charge-rich stripe form an antiferromagnetic order. As g decreases, E_t becomes lower. Correspondingly, the spin order is suppressed and it eventually disappears at $g = 0.6$. Since the lowest E_t is located at $g = 0.55$, the ground state is a nonmagnetic CO. This shows a qualitative difference with the MFA.^{19,20,23,27} Similarly, on the charge-poor sites (A' and C), a weak spin order is obtained for $g = 1$, which is also suppressed with decreasing g . The origin of this nonmagnetic state will be discussed in Sect. 3.3.

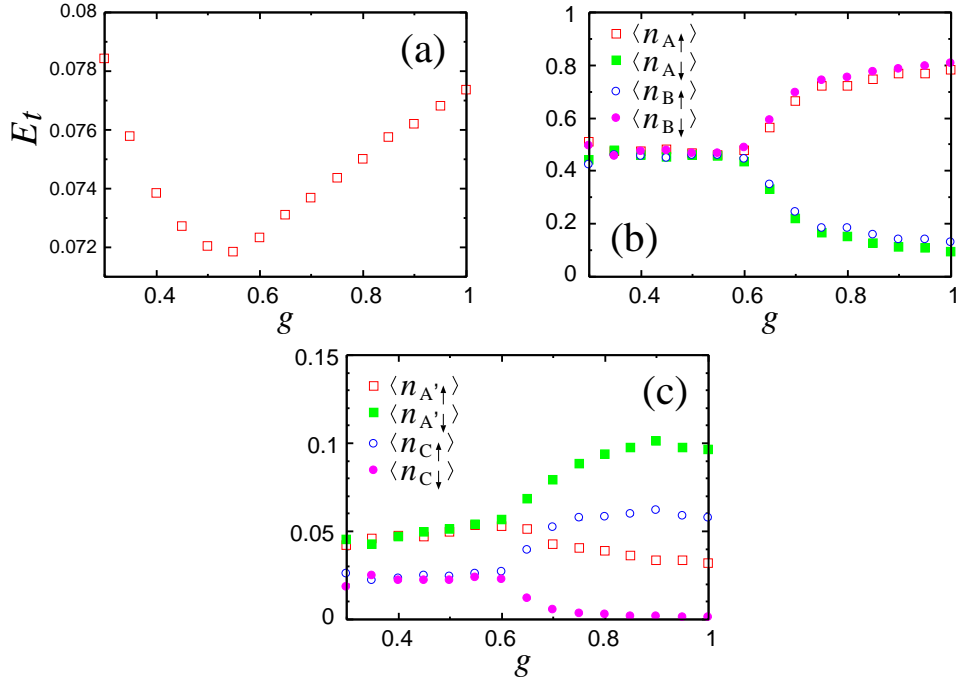


Fig. 2. (Color online) (a) Ground-state energy E_t , (b) average charge density $\langle n_{\alpha\sigma} \rangle$ for $\alpha = A, B$, and (c) those for $\alpha = A', C$ as a function of g with $w_a = w_b = 1$. We use $U = 0.7$, $V_a = 0.35$, $V_b = 0.25$, and $P = 0$ kbar.

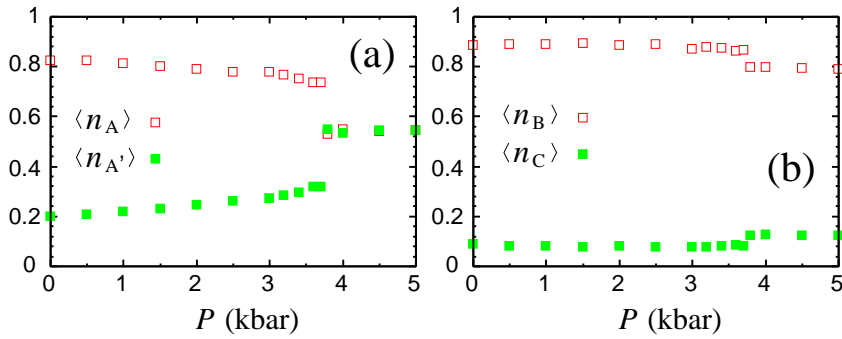


Fig. 3. (Color online) P dependence of (a) $\langle n_A \rangle$ and $\langle n_{A'} \rangle$, and (b) $\langle n_B \rangle$ and $\langle n_C \rangle$ with $U = 0.7$, $V_a = 0.35$, and $V_b = 0.25$.

3.2 Ground-state properties under uniaxial pressure

In the following, we show the fully optimized results with all the variational parameters. Note that the CO state is always nonmagnetic, which is in sharp contrast with the MFA.^{19,20,23,27} In Figs. 3(a) and 3(b), we plot $\langle n_\alpha \rangle$ ($= \langle n_{\alpha\uparrow} \rangle + \langle n_{\alpha\downarrow} \rangle$) as a function of the uniaxial pressure P (kbar). When $P = 0$ kbar, the ground state is the nonmagnetic CO. With increasing P , the charge disproportionation between the sites A and A' gradually decreases. At $P \sim 3.8$ kbar, there is a first-order transition where $\langle n_A \rangle$ and $\langle n_{A'} \rangle$ become equal, indicating

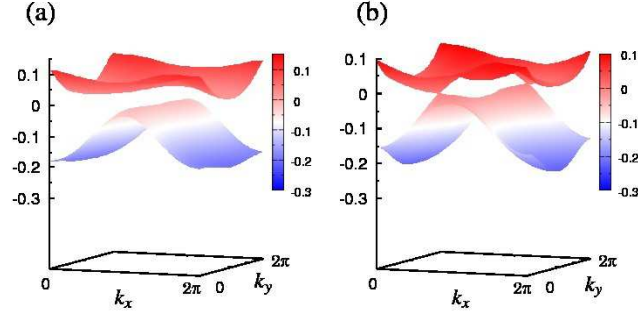


Fig. 4. (Color online) Energy dispersion of the lowest two bands for (a) $P = 0$ kbar and (b) $P = 5$ kbar. The other parameters are the same as those in Fig. 3. The Fermi energy is taken as zero.

a disappearance of the CO. For $P > 3.8$ kbar, the inversion symmetry that is broken by the CO is recovered. $\langle n_B \rangle$ and $\langle n_C \rangle$ are not affected by P except the transition point. They remain to be different through the transition since these sites are inequivalent in the crystal structure. The site B (C) is charge-rich (charge-poor) even in the noninteracting case.²²

In Figs. 4(a) and 4(b), we show the energy dispersion of the lowest two bands for $P = 0$ and 5 kbar, respectively. They are obtained by computing the eigenvalues of H^{MF} with sufficiently large system sizes, although the variational parameters are optimized with $N_u = 8 \times 8$. We confirmed that the results are qualitatively unchanged if the variational parameters with $N_u = 6 \times 6$ are employed. At $P = 0$ kbar, there is a charge gap because of the existence of CO. For $P = 5$ kbar, the energy dispersion indicates that a ZGS with two Dirac cones is realized. The Fermi level coincides with the contact points located at $\mathbf{k}_D^\pm = (\pm 0.70\pi, \pm 0.31\pi)$. The appearance of the Dirac cones by uniaxial pressure is consistent with the mean-field study.²³ The present result indicates that the renormalization of $\Delta_{\alpha\sigma}$ by electron correlation does not affect the Dirac cones qualitatively.

To investigate the correlation effects quantitatively, we consider the energy dispersion near the contact point. For α -I₃, the Dirac cone has a tilting and its dispersion is written as^{24, 28, 40, 45, 46}

$$\epsilon_{\mathbf{k}}^\pm = v_{x0}k_x + v_{y0}k_y \pm \sqrt{v_x^2k_x^2 + v_y^2k_y^2}, \quad (6)$$

where v_{x0} and v_{y0} are the velocities for the tilting, whereas v_x and v_y are those of the Dirac cone. Here, $\mathbf{k} = \mathbf{k}_D^\pm$ is taken as the origin. The degree of tilting is measured using the parameter η ($0 \leq \eta < 1$), which is defined as^{45, 46}

$$\eta = \sqrt{(v_{x0}/v_x)^2 + (v_{y0}/v_y)^2}. \quad (7)$$

We estimate η by fitting the obtained energy bands to Eq. (6) near $\mathbf{k} = \mathbf{k}_D^\pm$. The results are

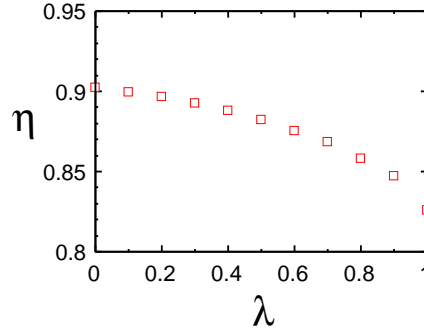


Fig. 5. λ dependence of the tilting parameter η at $P = 5$ kbar.

shown in Fig. 5 as a function of a parameter λ that controls the strength of the interactions. We set $U = 0.7\lambda$, $V_a = 0.35\lambda$, $V_b = 0.25\lambda$, and $P = 5$ kbar, where the ZGS is the ground state for $0 \leq \lambda \leq 1$. At $\lambda = 0$, we have $\eta \sim 0.9$. Although η gradually decreases with increasing λ , it is still larger than 0.8 at $\lambda = 1$. These values are consistent with those obtained in previous mean-field studies.^{28,40} For the values of v_x and v_y , they slightly decrease as λ increases. For example, we obtain $(v_x, v_y) = (0.0594, 0.0537)$ at $P = 0$ kbar and $(v_x, v_y) = (0.0527, 0.0495)$ at $P = 5$ kbar. Such a behavior is different from a recent renormalization group study with long-range Coulomb interactions,²⁹ where v_x and v_y show an enhancement near the contact point. The decrease in these velocities may come from the short-range Coulomb interactions considered in this study.

In Fig. 6, we show the phase diagram in the (P, V_b) plane for $U = 0.7$ and $V_a = 0.35$. The horizontal CO is dominant for small V_b . This is consistent with the MFA where the stabilities of various CO patterns are compared.^{19,20} The realization of the horizontal CO comes from its CO pattern that can avoid the energy loss by V_a as well as the band structure of α -I₃. As V_b increases, the horizontal CO is destabilized. This is considered to be due to charge frustration in a triangular lattice structure with $V_a \sim V_b$, which has been discussed for the case of θ -(BEDT-TTF)₂X.^{53,55,56} Furthermore, the uniaxial pressure P makes the CO unstable through the change in the band structure.²³ In the large P and V_b region, the ZGS appears. On the other hand, in the region with small P and large V_b , there is a metallic state that has electron Fermi surface and hole Fermi surface, which is basically the same as that in the noninteracting case at $P = 0$ kbar.²³

3.3 Origin of the nonmagnetic CO

To elucidate the origin of the nonmagnetic CO, we calculate the nearest-neighbor spin-spin correlation functions $\langle \mathbf{S}_\alpha \cdot \mathbf{S}_\beta \rangle_l$ as a function of P , where α and β indicate a pair of sites

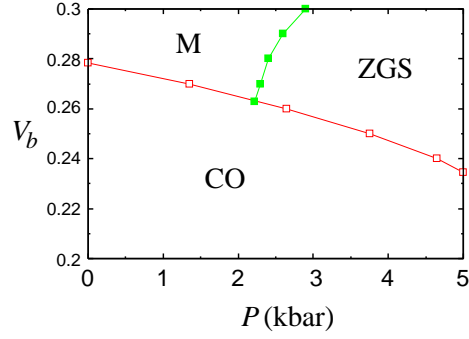


Fig. 6. Phase diagram on the (P, V_b) plane for $U = 0.7$ and $V_a = 0.35$, where M indicates a metallic state that has electron and hole pockets in the Fermi surface.

in the unit cell and l specifies the bond connecting these two sites. The results are shown in Fig. 7 for $l = b2$ and $b3$ (see Fig. 1). In the CO state for $P < 3.8$ kbar, the charge-rich stripe is found on the ABAB chain. On this charge-rich stripe, $|\langle \mathbf{S}_A \cdot \mathbf{S}_B \rangle_{b2}|$ is large while $|\langle \mathbf{S}_A \cdot \mathbf{S}_B \rangle_{b3}|$ is very small, which is reflected by the magnitude of t_{b2} and t_{b3} ($|t_{b2}| \sim 2|t_{b3}|$). This indicates that a spin-singlet is favored on the $b2$ bonds, which is markedly different from the results obtained in the MFA,^{19,20,23,27} but is consistent with the picture discussed from the NMR experiment.¹² We consider that a one-dimensional spin-Peierls system is essentially realized because of the correlation effects that are incorporated in the projection operators. In fact, when a spin-singlet is formed on the $b2$ bonds, we expect $\langle \mathbf{S}_A \cdot \mathbf{S}_B \rangle_{b2} \sim -\frac{3}{4} \langle n_A n_B \rangle_{b2}$ ^{57,58} since a charge-charge correlation function for the $b2$ bonds, $\langle n_A n_B \rangle_{b2}$, is the probability of occurrence for two electrons to occupy the nearest-neighbor sites A and B . Actually, at $P = 0$ kbar, we have $-\frac{3}{4} \langle n_A n_B \rangle_{b2} = -0.406$ and $\langle \mathbf{S}_A \cdot \mathbf{S}_B \rangle_{b2} = -0.348$ so that the result is consistent with the formation of the spin-singlet. Experimentally, there is a structural distortion at the CO transition, which slightly increases $|t_{b2}|$ on the charge-rich stripe, whereas t_{b3} is almost unchanged.¹¹ Although this may contribute to the spin-singlet formation, we consider that the lattice effect has only a minor role since the large bond alternation ($|t_{b2}| \sim 2|t_{b3}|$) already exists in the metallic phase.

For $P > 3.8$ kbar, the CO disappears and the sites A and A' become equivalent. An antiferromagnetic correlation exists on the two $b2$ bonds that connect a set of three sites A , A' , and B . $\langle \mathbf{S}_\alpha \cdot \mathbf{S}_\beta \rangle_l$ are almost constant as a function of P in the ZGS.

On the other hand, $|\langle \mathbf{S}_\alpha \cdot \mathbf{S}_\beta \rangle_{b1}|$ (not shown) is small although $|t_{b1}|$ is large. This is because the site C is always charge-poor so that the spin-spin correlation does not develop on the $b1$ bonds.

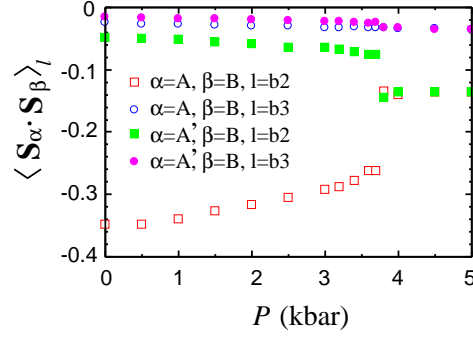


Fig. 7. (Color online) P dependence of the nearest-neighbor spin-spin correlation functions $\langle \mathbf{S}_\alpha \cdot \mathbf{S}_\beta \rangle_l$ for $l = b2$ and $b3$. The other parameters are the same as those in Fig. 3.

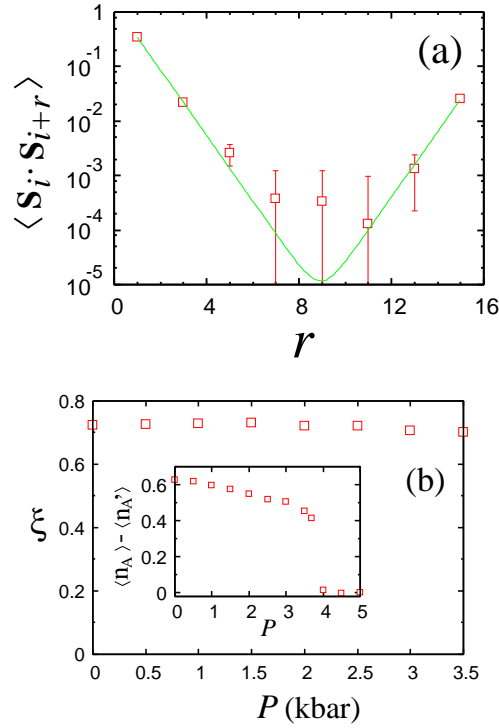


Fig. 8. (a) r dependence of $\langle \mathbf{S}_i \cdot \mathbf{S}_{i+r} \rangle$ with $i = A$ at $P = 0$ kbar and (b) the spin correlation length ξ as a function of P . The inset shows the difference between the average charge densities on the sites A and A' . The other parameters are the same as those in Fig. 3.

3.4 Spin gap and CO

Finally, we discuss the spin gap in the CO state. Figure 8(a) shows the long-distance behavior of the spin-spin correlation function $\langle \mathbf{S}_i \cdot \mathbf{S}_{i+r} \rangle$ along the charge-rich stripe at $P = 0$ kbar, where we set $i = A$ and the distance r is measured along the stripe. Since the spin-gap

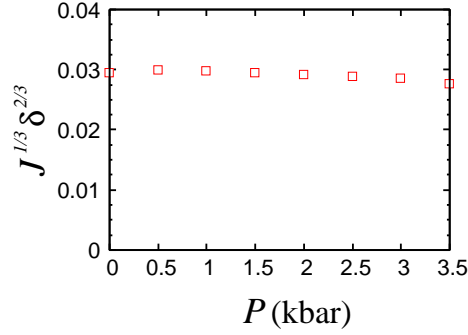


Fig. 9. $J^{1/3} \delta^{2/3}$ as a function of P .

behavior appears as an exponential decay of $\langle \mathbf{S}_i \cdot \mathbf{S}_{i+r} \rangle$, we fit the results as

$$\langle \mathbf{S}_i \cdot \mathbf{S}_{i+r} \rangle = c_1 e^{-r/\xi} + c_2 e^{-(L-r)/\xi}, \quad (8)$$

where c_1 , c_2 , and the spin correlation length ξ are fitting parameters. The fitting curve is also depicted in Fig. 8(a). The result is in fact consistent with the existence of the spin gap. As shown in Fig. 8(b), ξ is almost constant as a function of P indicating that the spin gap Δ_s has very weak P dependence if we assume $\Delta_s \propto \xi^{-1}$. This behavior is in contrast to the suppression of the CO, which is manifested by a decrease in $\langle n_A \rangle - \langle n_{A'} \rangle$, as shown in the inset. We note that the P dependence of ξ is also weaker than that of the nearest-neighbor spin-spin correlation function $\langle \mathbf{S}_A \cdot \mathbf{S}_B \rangle_{b2}$. Their pressure dependences are in general different from each other since ξ is determined by the long-range correlation functions.

4. Discussion

Actually, recent transport and NMR measurements^{48,49} have revealed that the spin gap is robust against hydrostatic pressure even in the region where T_{CO} and the charge gap are largely suppressed.

In order to understand the reason why Δ_s is roughly independent of P , we estimate Δ_s from another viewpoint. We regard the ABAB chain in the CO state as a one-dimensional spin system. Then, the effective spin exchange coupling on the b2 bonds is written as $J_{b2} \sim 4t_{b2}^2 \langle n_A n_B \rangle_{b2} / U$, whereas that on the b3 bonds is given by $J_{b3} \sim 4t_{b3}^2 \langle n_A n_B \rangle_{b3} / U$.^{57,58} Therefore, this spin system can be regarded as a Heisenberg spin chain with alternating exchange couplings, J_{b2} and J_{b3} . This model has a spin gap $\Delta_s \propto J^{1/3} \delta^{2/3}$, where $J = (J_{b2} + J_{b3})/2$ and $\delta = (J_{b2} - J_{b3})/2$.^{59,60} In Fig. 9, we plot $J^{1/3} \delta^{2/3}$ as a function of P . Apparently, the P dependence of Δ_s is very weak and this estimation is consistent with the behavior of ξ in Fig. 8. The physical reason is as follows. When we increase P , $|t_{b2}|$ and $|t_{b3}|$ increase. However,

$\langle n_A n_B \rangle_{b2}$ and $\langle n_A n_B \rangle_{b3}$ decrease with P because of the suppression of the CO, the effect of which nearly cancels with the above enhancement.

Finally, we remark on the difference between uniaxial and hydrostatic pressures. The latter has been used in several experiments such as NMR^{48,49} and Raman¹⁰ studies. Because the hydrostatic pressure essentially increases transfer integrals uniformly, its main effect is to increase the bandwidth.⁶¹ On the other hand, the change in transfer integrals is more anisotropic for the case of uniaxial pressure.²² Although the CO insulating state changes into the ZGS for both cases,¹⁵ there appear some differences in electronic properties: (i) T_{CO} has only weak pressure dependence under uniaxial pressure compared with that under hydrostatic pressure.¹⁵ (ii) Theoretically, it has been suggested that the effects of anion potentials may be important for the appearance of the ZGS under hydrostatic pressure,²⁵ which is different from the case of uniaxial pressure where it emerges even without the anion potentials. We expect that these differences do not have a significant role in the pressure dependence of spin and charge degrees of freedom obtained in this paper because of the following reasons. Experimentally, the resistivity under uniaxial pressure shows a substantial decrease as a function of pressure for $T < T_{CO}$, indicating that the CO is suppressed as in the case of hydrostatic pressure. In fact, at $T = 0$, our results on $\langle n_A \rangle - \langle n_{A'} \rangle$ show that it gradually decreases and vanishes discontinuously at a critical pressure, as shown in Fig. 8(b). This is qualitatively consistent with the estimation from Raman experiments under hydrostatic pressure.¹⁰ Therefore, we consider that point (i) does not affect our results essentially. The consistency between our results and the Raman experiments also suggests that the anion potentials do not have a major role in the pressure dependence of the CO so that point (ii) will not be important at least in the CO state.

For the spin gap, we consider that its weak pressure dependence is basically unaltered even when we take account of the hydrostatic pressure, because the hydrostatic pressure also induces the suppression of the CO together with the increase in the transfer integrals along the charge-rich stripe. As discussed in the present paper, these effects lead to the weak pressure dependence of Δ_s compared with the charge degrees of freedom. These considerations support the applicability of the present calculations to the experimental results under hydrostatic pressure.

5. Summary

In this paper, we investigate correlation effects on the ground-state properties in the organic conductor α -I₃. In the CO state, we have shown that the antiferromagnetic spin order

that is predicted by the MFA disappears owing to the correlation effects. The spins on the charge-rich stripe tend to form a spin-singlet on the bonds with large transfer integrals. Under uniaxial pressure, there is a transition from the nonmagnetic CO to the ZGS. We suggest that the uniaxial pressure dependence of the spin gap is very weak compared with that of the CO. These different behaviors in the spin and charge degrees of freedom are qualitatively consistent with experimental observations.

Acknowledgments

Y. T. is grateful to H. Watanabe for fruitful discussions. The authors would like to thank D. Liu, K. Miyagawa, and K. Kanoda for helpful discussions.

References

- 1) T. Ishiguro, K. Yamaji, and G. Saito, *Organic Superconductors* (Springer-Verlag, Berlin, 1998) 2nd ed.
- 2) H. Seo, C. Hotta, and H. Fukuyama, *Chem. Rev.* **104**, 5005 (2004).
- 3) K. Kajita, Y. Nishio, N. Tajima, Y. Suzumura, and A. Kobayashi, *J. Phys. Soc. Jpn.* **83**, 072002 (2014).
- 4) K. Bender, K. Dietz, H. Enders, H. W. Helberg, I. Hennig, H. J. Keller, H. W. Schafer, and D. Schweitzer, *Mol. Cryst. Liq. Cryst.* **107**, 45 (1984).
- 5) C. P. Heidmann, A. Bansteiner, F. Gross-Alltag, B. S. Chandrasekhar, and E. Hess, *Solid State Commun.* **84**, 711 (1992).
- 6) T. J. Emge, P. C. W. Leung, M. A. Beno, H. H. Wang, and J. M. Williams, *Mol. Cryst. Liq. Cryst.* **138**, 393 (1986).
- 7) N. A. Fortune, K. Murata, M. Ishibashi, M. Tokumoto, N. Kinoshita, and H. Anzai, *Solid State Commun.* **79**, 265 (1991).
- 8) Y. Takano, H. M. Yamamoto, K. Hiraki, T. Nakamura, and T. Takahashi, *J. Phys. Chem. Solids* **62**, 393 (2001).
- 9) Y. Takano, K. Hiraki, H. M. Yamamoto, T. Nakamura, and T. Takahashi, *Synth. Met.* **120**, 1081 (2001).
- 10) R. Wojciechowski, K. Yamamoto, K. Yakushi, M. Inokuchi, and A. Kawamoto, *Phys. Rev. B* **67**, 224105 (2003).
- 11) T. Kakiuchi, Y. Wakabayashi, H. Sawa, T. Takahashi, and T. Nakamura, *J. Phys. Soc. Jpn.* **76**, 113702 (2007).
- 12) T. Kawai and A. Kawamoto, *J. Phys. Soc. Jpn.* **78**, 074711 (2009).
- 13) Y. Yue, K. Yamamoto, M. Uruichi, C. Nakano, K. Yakushi, S. Yamada, T. Hiejima, and A. Kawamoto, *Phys. Rev. B* **82**, 075134 (2010).
- 14) B. Rothaemel, L. Forro, J. R. Cooper, J. S. Schilling, M. Weger, P. Bele, H. Brunner, D. Schweitzer, and H. J. Keller, *Phys. Rev. B* **34**, 704 (1986).
- 15) N. Tajima, S. Sugawara, M. Tamura, Y. Nishio, and K. Kajita, *J. Phys. Soc. Jpn.* **75**, 051010 (2006).
- 16) S. Katayama, A. Kobayashi, and Y. Suzumura, *J. Phys. Soc. Jpn.* **75**, 054705 (2006).
- 17) H. Kino and H. Fukuyama, *J. Phys. Soc. Jpn.* **64**, 1877 (1995).

- 18) H. Kino and H. Fukuyama, J. Phys. Soc. Jpn. **65**, 2158 (1996).
- 19) H. Seo, J. Phys. Soc. Jpn. **69**, 805 (2000).
- 20) Y. Tanaka and K. Yonemitsu, J. Phys. Soc. Jpn. **77**, 034708 (2008).
- 21) S. Miyashita and K. Yonemitsu, J. Phys. Soc. Jpn. **77**, 094712 (2008).
- 22) A. Kobayashi, S. Katayama, K. Noguchi, and Y. Suzumura, J. Phys. Soc. Jpn. **73**, 3135 (2004).
- 23) A. Kobayashi, S. Katayama, and Y. Suzumura, J. Phys. Soc. Jpn. **74**, 2897 (2005).
- 24) A. Kobayashi, S. Katayama, Y. Suzumura, and H. Fukuyama, J. Phys. Soc. Jpn. **76**, 034711 (2007).
- 25) Y. Suzumura, and A. Kobayashi, J. Phys. Soc. Jpn. **82**, 044709 (2013).
- 26) A. Kobayashi and Y. Suzumura, J. Phys. Soc. Jpn. **82**, 054715 (2013).
- 27) A. Kobayashi, Y. Suzumura, F. Piechon, and G. Montambaux, Phys. Rev. B **84**, 075450 (2011).
- 28) S. Katayama, A. Kobayashi, and A. Suzumura, Eur. Phys. J. B **67**, 139 (2009).
- 29) H. Isobe and N. Nagaosa, J. Phys. Soc. Jpn. **81**, 113704 (2012).
- 30) A. Kobayashi, S. Komaba, S. Katayama, and Y. Suzumura, J. Phys. Conf. Ser. **132**, 012002 (2008).
- 31) A. Kobayashi, S. Katayama, and Y. Suzumura, Sci. Adv. Mater. **10**, 024309 (2009).
- 32) M. O. Goerbig, J. -N. Fuchs, G. Montambaux, and F. Piechon, Phys. Rev. B **78**, 045415 (2008).
- 33) T. Morinari and Y. Suzumura, J. Phys. Soc. Jpn. **83**, 094701 (2014).
- 34) F. Piechon and Y. Suzumura, J. Phys. Soc. Jpn. **82**, 123703 (2013).
- 35) M. Monteverde, M. O. Goerbig, P. Auban-Senzier, F. Navarin, H. Henck, C. R. Pasquier, C. Mézière, and P. Batail, Phys. Rev. B **87**, 245110 (2013).
- 36) T. Mori, J. Phys. Soc. Jpn. **82**, 034712 (2013).
- 37) F. Piechon and Y. Suzumura, J. Phys. Soc. Jpn. **82**, 033703 (2013).
- 38) Y. Suzumura, T. Morinari, and F. Piechon, J. Phys. Soc. Jpn. **82**, 023708 (2013).
- 39) T. Nishine, A. Kobayashi, and Y. Suzumura, J. Phys. Soc. Jpn. **79**, 114715 (2010).
- 40) A. Kobayashi, Y. Suzumura, and H. Fukuyama, J. Phys. Soc. Jpn. **77**, 064718 (2008).

- 41) A. Kobayashi, Y. Suzumura, H. Fukuyama, and M. O. Goerbig, *J. Phys. Soc. Jpn.* **78**, 114711 (2009).
- 42) H. Kino and T. Miyazaki, *J. Phys. Soc. Jpn.* **75**, 034704 (2006).
- 43) Y. Suzumura and A. Kobayashi, *J. Phys. Soc. Jpn.* **80**, 104701 (2011).
- 44) I. Proskurin and M. Ogata, *J. Phys. Soc. Jpn.* **82**, 063712 (2013).
- 45) Y. Suzumura, I. Proskurin, and M. Ogata, *J. Phys. Soc. Jpn.* **83**, 023701 (2014).
- 46) Y. Suzumura, I. Proskurin, and M. Ogata, *J. Phys. Soc. Jpn.* **83**, 094705 (2014).
- 47) M. Hirata, K. Ishikawa, K. Miyagawa, K. Kanoda, and M. Tamura, *Phys. Rev. B* **84**, 125133 (2011).
- 48) D. Liu, Dr. Thesis, Faculty of Engineering, University of Tokyo, Tokyo (2016).
- 49) D. Liu, K. Ishikawa, R. Takehara, K. Miyagawa, M. Tamura, and K. Kanoda, *Phys. Rev. Lett.* **116**, 226401 (2016).
- 50) H. Yokoyama and H. Shiba, *J. Phys. Soc. Jpn.* **59**, 3669 (1990).
- 51) H. Yokoyama, Y. Tanaka, M. Ogata, and H. Tsuchiura, *J. Phys. Soc. Jpn.* **73**, 1119 (2004).
- 52) H. Watanabe and M. Ogata, *J. Phys. Soc. Jpn.* **74**, 2901 (2005).
- 53) H. Watanabe and M. Ogata, *J. Phys. Soc. Jpn.* **75**, 063702 (2006).
- 54) S. Sorella, *Phys. Rev. B* **64**, 024512 (2001).
- 55) J. Merino, H. Seo, and M. Ogata, *Phys. Rev. B* **71**, 125111 (2005).
- 56) S. Nishimoto, M. Shingai, and Y. Ohta, *Phys. Rev. B* **78**, 035113 (2008).
- 57) M. Ogata and H. Shiba, *Phys. Rev. B* **41**, 2326 (1990).
- 58) Y. Tanaka and M. Ogata, *J. Phys. Soc. Jpn.* **74**, 3283 (2005).
- 59) M. C. Corss and D. S. Fisher, *Phys. Rev. B* **19**, 402 (1979).
- 60) E. Orignac, *Eur. Phys. J. B* **39**, 335 (2004).
- 61) R. Kondo, S. Kagoshima, N. Tajima, and R. Kato, *J. Phys. Soc. Jpn.* **78**, 114714 (2009).